Quartz Capillary Microreactor for Studies of Oxidation in Supercritical Water

Sean P. Maharrey and David R. Miller
Chemical Engineering Program, Dept. of Mechanical and Aerospace Engineering, University of California, San Diego, La Jolla, CA 92093

An inexpensive, low-power quartz capillary flow reactor was designed to investigate the global reaction rate for the supercritical water oxidation of acetic acid. The effluent from the ~0.1 cm dia. quartz microreactor is such that it is easily incorporated into an online spectroscopic or vacuum mass spectrometer detection system. The reactor is capable of operating up to 28 MPa and 530°C. Standard HPLC sample injection valves permit the rapid change of reactant composition. This reactor is a nonisothermal design and requires a heat-transfer calculation that involves coupling the transport equations for momentum, mass, and heat with the chemical kinetics equations. A numerical calculation presented includes a rigorous treatment of the equation of state and the transport properties of pure water. With this design, the global rate data was fitted to the following form: $r_A = -9.3 \pm 0.7 \times 10^{10} e^{-(172.2 \pm 1.7)/RT} [C_{HOAc}]^{0.89 \pm 0.07} [C_{Peroxide}]^{0.2 \pm 0.1}$*(M/s).*

Introduction

Supercritical water oxidation (SCWO) is a relatively new technology for the destruction of toxic organic wastes. The organic contaminant and oxidizer are both completely miscible with supercritical (SC) water, and the resulting single-phase reaction environment supports a very efficient oxidation reaction, >99% completion, and minimizes the formation of equally harmful byproducts. In order to scale up existing bench-scale reactors to full-scale facilities, the oxidation kinetics of a given oxidation reaction must be well understood. (Modell (1989), Tester et al. (1993), *Haz. Waste Consult.* (1999), and Schmieder and Abeln (1999) give reviews of SCWO technology.) Aki and Abraham (1998), Cansell et al. (1998), and Rice and Steeper (1998) give results for the oxidation kinetics of model industrial compounds in SCWO.

Current reactor designs used for SCWO are generally based on closed-loop flow reactors on the order of meters in length. These designs use individual preheat sections for the reactants and SC water, which are then mixed and enter the flow reactor where the reaction initiates and proceeds. After exiting the flow reactor, the mixture enters a heat exchanger followed by an expansion valve, which together act to reduce the temperature and pressure of the SC mixture and also quench the oxidation reaction. The valve expands the flow into a large recovery vessel held at atmospheric pressure, which results in flow separation and the corresponding recovery of both liquid and gas-phase reactor effluent. The recovered liquid-phase is generally sampled and analyzed by HPLC, while GC is used for the gas phase. An example of this type of reactor design is that used by Tester and his group at MIT (Holgate and Tester, 1993).

The large scale of these reactor designs often requires significant power to operate at supercritical conditions, on the order of a few kW. With their large size and high power requirements, these reactors do not adjust rapidly to changes in reactor conditions, requiring several minutes to reach a new steady state for a new set of flow conditions. Further, the closed-loop design means that a reactant mixture must be loaded and sealed into a sample reservoir before the unit is started. This sample loading technique means that only a single reactant mixture can be studied for a given reactor run. There is also a large turnaround time for these designs. The HPLC and GC techniques for analyzing the reactor effluent are limited in that they can only detect remaining reactants and stable product species, unstable and short-lived intermediates, and radicals are not observed with these techniques. Finally, the temperature and pressure reduction process has a typical residence time on the order of seconds, not necessarily favorable conditions for quenching the oxidation reac-

Correspondence concerning this article should be addressed to S. P. Maharrey at this current address: Sandia National Laboratories, P.O. Box 969, MS-9052, Livermore, CA 94551-0969.

tion. Second-generation flow reactor designs incorporate optical diagnostics directly into the heated zone of the reactor and have been able to observe a limited number of intermediate species (Brown and Steeper, 1991; Myrick et al., 1994; Rice et al., 1996).

Our objective was to design an inexpensive microreactor that could be incorporated directly into a spectroscopic or vacuum mass spectrometer detection system in order to analyze online the reactant/intermediate/product mixture. We followed the lead of Groeger and Fenn (1988), who designed a microflow reactor that served simultaneously as a standard molecular beam free-jet source that easily permitted FTIR spectroscopic detection. We were especially interested in using a direct sampling mass spectrometry (DSMS) system to analyze the reactive agents and products present in the supercritical reaction mixture, and their approach was ideal for this purpose. Other studies using a supersonic jet molecular beam interface to couple a supercritical fluid chromatograph to a mass spectrometer for product identification were conducted by Randall and Wahrhaftig (1978, 1981), Fukuoka et al. (1986), Syage (1990), Smith et al. (1986), and Lustig and Lubman (1991). These studies were also useful in the development of our design to incorporate DSMS. The incorporation of this reactor design into a DSMS system and the detection scheme for radicals and unstable intermediates in the overall oxidation reaction will be presented elsewhere (Maharrey and Miller, 2001). In this article we wish to show that the micro reactor design is useful and permits a rapid survey of overall kinetic parameters, using the apparatus as a benchtop flow reactor.

We report the design of the quartz capillary microflow reactor and high-pressure water delivery system that can be used with supercritical water. This reactor design significantly reduces the power density of the previous designs to levels below 100 Ws. Included in this design is a sample injection port that allows introduction of initial sample mixtures while the reactor in operating under a given set of conditions. This sample introduction technique eliminates the need to shut down the reactor in order to change the reactant mixture being used for a given run. With the small scale and low power density, the reactor also rapidly responds to changes in flow conditions. This reactor was operated on the benchtop and because the important experimental inlet variables pressure, temperature, composition, and flow rate can be very efficiently manipulated, the global reaction parameters can be rapidly developed. In these studies, the entire reactor effluent is captured to investigate the global reaction rate for the SCWO of a given reactant.

With its low power, low cost, small flow rates, and simple pumping system, this microflow reactor design provides a flexible, maintainable, and easy to operate platform with which to investigate the oxidation of organics in supercritical water. We chose to use acetic acid as our prototypical reactant to demonstrate the validity of the reactor design. Acetic acid was initially thought to be a major intermediate in the overall oxidation of larger molecular weight hydrocarbons and was also considered to be a rate-limiting step in the overall oxidation (Lee et al., 1990). There were conflicts with this result, however (Wightman, 1981; Rice et al., 1993). We also chose hydrogen peroxide over oxygen as our oxidizer. This was simply due to experimental convenience. Hydrogen peroxide can be obtained as an aqueous solution as strong as 30 wt. % and allows easy sample preparation, as well as an accurate determination of the initial oxidizer concentration.

Experimental Design

A detailed description of the experimental design can be found elsewhere (Maharrey, 1998). Figure 1 shows the overall design, consisting of the high-pressure delivery system and the capillary quartz reactor. In addition to its micro scale, there are two important components of this otherwise straightforward flow-reactor system. The flow exits the reactor through a very small converging sonic nozzle. In this section, the flow accelerates to a Mach number (flow velocity divided by the local speed of sound) of $M = 1$, and then undergoes a free-jet expansion into either the ambient background or into a vacuum, depending on the detection scheme to be used. In addition, there is a separate nitrogen gas flow path that is used to both purge the system and to calibrate the critical exit nozzle diameter before and after each run. This is necessary because the small exit nozzle properties control the flow rate in the reactor for given upstream conditions, and it is necessary to verify that the nozzle has neither clogged nor has been eroded away, as may happen in the case of SCW.

Shown in Figure 1 is the (1) Varian model 8500 high-pressure liquid-chromatography piston-syringe pump, (2) a Valco model 212UWHC switching valve, (3) an Omega model PX602 pressure transducer, (4) a secondary nitrogen flow loop and calibration volume, and (5) the quartz capillary reactor and

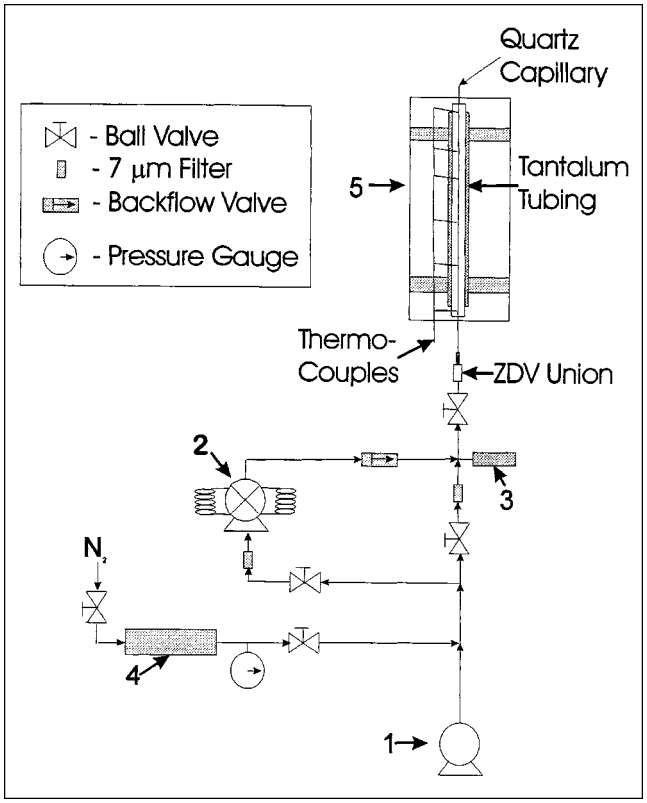

Figure 1. High-pressure water delivery system and quartz capillary reactor assembly.

heater assembly. The Varian pump gives very accurate and reproducible flow rates of high-pressure water/reactant mixtures from 10–990 mL/h and gives us from 2–3 h of continuous steady-state runtime at our flow rates using a single pump loading of 250 mL of water. Sample injection is done with the Valco switching valve which contains two 10 mL sample loops, loaded through syringe adapters, and gives us the ability to inject initial reactant mixtures directly into the high-pressure water flow, while operating the reactor at a predetermined steady state. Reactor inlet pressure is monitored during the course of a run with the Omega pressure transducer, which also allows us to monitor the approach to steady state while heating the reactor to a given temperature.

The nitrogen secondary flow path, which bypasses the sample valve and includes a calibrated volume, can be brought online by appropriate valves and allows for purging the reactor with nitrogen at the end of a set of experimental runs. Further, by applying the equation for compressible choked flow through the sonic exit nozzle, relating the nitrogen gas pressure inside the calibrated volume to the mass flow rate of the gas out of the nozzle, the diameter of the nozzle can be calculated. We verify the diameter of the nozzle by this technique both before and after each experimental run.

This high-pressure delivery system is connected to the quartz reactor assembly with PEEK (poly-ethyl-ethyl ketone) flexible tubing and standard HPLC stainless steel compression fittings. The PEEK tubing is connected to the capillary quartz using a PEEK capillary sleeve in an HPLC zero-dead volume (ZDV) compression fitting. PEEK tubing is 0.1588 cm OD with a 0.0508 cm ID, while the capillary sleeves are 0.1588 cm OD with a 0.0762 cm ID, which can be reamed-out to allow coupling to larger diameter quartz tubing. These fittings and PEEK tubing are all available from Upchurch Scientific of Oak Harbor, WA. All fittings are 304 stainless steel compression fittings and all tubing is 0.3175 cm OD 316 stainless steel with 0.1245 cm wall thickness. Whitney SS-83KS4 ball valves are used to isolate each section. The sample loops on the Valco switching valve are 0.3175 cm OD 316 stainless steel with a 0.1524 cm ID. Total length of stainless steel tubing is 757 cm for the line including the sample loops and 133 cm for the line including the calibrated volume.

The quartz reactor assembly consists of a 33 cm long segment of quartz capillary tubing housed within a 20 cm long segment of tantalum tubing (0.254 cm OD, 0.0051 cm wall thickness). The internal diameter of the capillary quartz reactor is typically 0.075 cm (750 μm). A short converging section ending with a small diameter nozzle terminates the quartz reactor and chokes the flow to maintain a constant flow rate for a given temperature and pressure condition. The tantalum is resistively heated and is held within a ceramic tube for thermal insulation. The quartz is held centered in the tantalum by ceramic standoffs mounted in each end of the tantalum. Temperature is measured by six chromel-alumel thermocouples equally spaced along the outer wall of the quartz. Power is connected to the tantalum by the use of a copper barrel and braid concentration at the reactor inlet end and by 20 gauge nichrome loops at the outlet end. The nichrome is used on the outlet to allow us to keep this connection slightly hotter than the underlying tantalum to prevent the connection from becoming a heat sink. Copper rods (0.635 cm diameter, 35 cm long) are used to bring power into the reactor assembly and double as the support for all reactor components. Control of the power supplied to the reactor is obtained by connecting the thermocouple at the reactor outlet end of the quartz to an Omega model 50 temperature controller. A nitrogen purge is included in the reactor design to sweep out any oxygen present in the background and minimize oxidation of the hot metal parts used for power delivery. This complete quartz reactor assembly is then mounted within an aluminum tube (5.72 cm OD, 5.1 cm ID), which is used as a mechanical support for the assembly, and as a point of attachment for rigidly mounting the reactor assembly during experiments. The internal volume of the reactor assembly is packed with glass wool to minimize heat loss to the aluminum tube. A brass endcap completes the assembly and contains the insulated feedthroughs for power, nitrogen, and fluid delivery. A HP Vectra 386 computer using a Data Translation DT2805 A/D card logs all temperature, pressure, and power data. Programming for the A/D card was done in-house.

A mini-torch, using a methane/oxygen gas mixture, is used to melt the tip of the quartz down to the desired nozzle exit diameter, typically of order 0.002 cm (20 μm) in diameter. This process generates a converging section that is terminated by the nozzle. Typically, this converging nozzle section is $\sim$3 quartz capillary diameters in length. The quartz capillary is obtained from Polymicro Technologies of Phoenix, AZ, and we primarily use the 700 μm ID/850 μm OD tubing that is sheathed with a 15 μm polyimide coating.

For the global rate experiments reported here, the entire reactor effluent was captured. The reactor effluent collection vessel consisted of a short Pyrex tube with a 5° slope to its front face and an 85° elbow in the middle and necking down to a small ''drain.'' The 5° slope to the front face insured that when this tube was butted-up to the reactor exit, there was a downward slope to prevent collected water from pooling-up and not draining. This vessel was then wrapped with surgical gauze and continuously wetted with methanol. Small sample collection bottles were placed at the bottom of the drain to collect aliquots of the effluent for testing or for collecting the entire run for mass recovery analysis. With this design, mass recovery was $>$ 95%.

Determination of the acetic acid concentration both before and after flowing through the reactor was accomplished by using standard acid/base titration with phenolphthalein as the indicator and standardized and diluted (10^{-4} and 10^{-5} normal) NaOH as the base. All chemicals used for the titrations were standardized HCl, NaOH, and phenolphthalein obtained from Fisher Scientific (No. SA48-1, No. SS266-1, and No. P79-100, respectively). Acetic acid and hydrogen peroxide were also obtained from Fisher (No. A38^{S}-500 and No. H325-500), with the acetic acid obtained as glacial ($>$99%) and the hydrogen peroxide as a $\sim$30 wt. % solution in water. Ultra pure water was used as the source for all water and was made by distilling deionized water in a Corning Mega-Pure System model MP-3A still.

Reactor Analysis

As mentioned above, one caveat of this reactor design is that it is not isothermal. Furthermore, using such small capillaries does not permit a direct measurement of the supercriti-

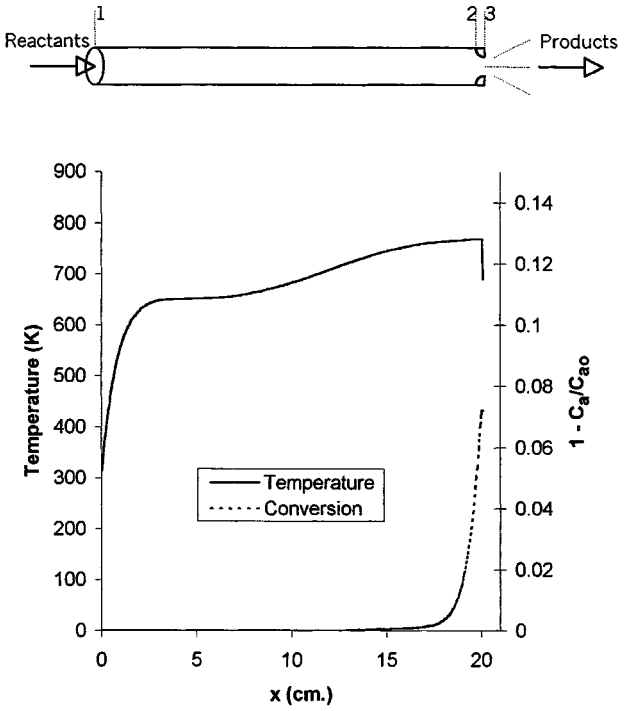

$$CH_3COOH + 4H_2O_2 \rightarrow 2CO_2 + 6H_2O$$

$P_0 = 23$ MPa, $\dot{Q} = 60$ ml/hr, $T_{02} = 490^{\circ}C$, $D_N = 20.3$ μm,
$C_{ao} = 8.3 \bullet 10^{-4}$ g/L, $C_{zo} = 2.4 \bullet 10^{-4}$ g/L

	1	1-2	2-3	3-Products
Re	400	1200	10^5	-
τ (s)	-	3	$5 \bullet 10^{-4}$	$10 \bullet 10^{-6}$

Figure 2. Reactor simulation.

cal water temperature as it flows through the reactor. This design limitation complicates the analysis of the experimental data when calculating the kinetic parameters in the global rate law for the oxidation of acetic acid. We therefore developed a heat-transfer model that coupled the heat transfer, thermodynamics, and kinetics for the SCWO of acetic acid. The details of the numerical solutions are available elsewhere (Maharrey, 1998).

The insert in Figure 2 shows the reactor and three associated flow regimes, the constant area heating section (1-2) where the reactants are heated and reaction occurs, the converging nozzle section (2-3) where the flow accelerates and compressibility effects are important near the sonic exit, and the supersonic expansion section (3 and beyond). The equations given below are valid for the entire reactor and nozzle (1-3). Our numerical code was not stable for the entire compressible flow regime up to Mach number $M = 1$. However, we were able to compute the flow up to $M = 0.9$ and show that the flow in the converging section beyond $M = 0.3$ became nearly isentropic with negligible transport effects and that the chemistry was completely quenched beyond this point.

The model was therefore separated into two distinct regions. Region 1 is effectively incompressible flow and consists of the constant area reactor region and the entrance portion of the converging nozzle region up to $M = 0.3$. Region 2 is compressible flow and extends from $M = 0.3$ up to the nozzle exit, where $M = 1.0$. In region 1, the full set of equations shown below is solved down the length of the reactor. Region 2 is a high-speed compressible flow region, and we used the isentropic, compressible flow model to calculate the reactor conditions in this region. The chemical kinetics equations are not coupled into the isentropic flow region, as there are no chemical reactions taking place in this region due to its short residence time, on the order of 10^{-3} s, and rapid temperature and pressure reduction, which act to quench the reaction.

Two major assumptions were made in developing the model used for region 1 of the reactor. The first was that the flow was essentially quasi-one-dimensional, which gives significant simplification in the transport equations. Evaluating the critical parameters given by Cutler et al. (1988) for the applicability of a plug-flow model to our tubular flow reactor, we found that we were well within the bounds for assuming negligible axial diffusion, but were only borderline on the assumption of negligible radial diffusion. For these calculations, we used values for diffusion coefficients that were valid for general hydrocarbon/water solutions at ambient conditions and then applied empirical correlations, obtained from Bird et al. (1960), to correct the temperature and pressure. The following is the quasi-one-dimensional compressible flow model used for the analysis of the global rate law experiments in this tubular reactor.

Conservation of Mass:

$$\rho V A_t = \dot{m}$$

Conservation of Species:

$$D\rho_i/Dt = V(d\rho_i/dx) = \nu_i M_i r_A$$

Conservation of Momentum:

$$dP + \rho V dV = -\left(\rho V^2 f_r/2\right)(4dx/D_i)$$

where f_r is the friction coefficient and is given by standard correlations (Bird, 1960)

$$f_r = 16/Re \ (Re < 2{,}000, \text{ laminar flow})$$

$$f_r = 0.0791/Re^{0.25} (Re > 2{,}000, \text{ turbulent flow})$$

Conservation of Energy:

$$dh + VdV = \left[(U_T/\rho V D_i)(T_w(x) - T) + \left(V^2 f_r/2\right)\right](4dx/D_i) - (r_A \Delta H_R(T)/\rho V)(dx)$$

where U_T is the overall heat-transfer coefficient and is given by the corresponding correlation, also from Bird (1960)

$$U_T = \left[1/Nu \cdot k_f + \ln(D_o/D_i)/2k_s\right]^{-1}$$

where Nu is the fluid Nusselt number. We initially used the value for fully developed flow in a circular tube with constant wall temperature $Nu = 3.66$ (Arpaci and Larsen, 1984). Later, we found a rigorous correlation for the Nu for forced convection heat transfer to supercritical water in a circular tube (Yamagata et al., 1972). When we reanalyzed our earlier pure water runs with Yamagata's Nu correlation, the reactor outlet temperature changed by less than 5°C and we therefore retained the simpler $Nu = 3.66$ value for our model.

Equation of State:

$$P = P(\rho, T) \quad h = h(\rho, T) \quad s = s(\rho, T) \quad a_s = a_s(\rho, T)$$

where a_s is the speed of sound of the fluid. The second major assumption made is that the reactant mixtures were dilute and the thermodynamics can be given by an equation of state for pure water. From the range of thermodynamic conditions encountered in an experiment, this assumption still required a rigorous equation of state for water, and we used the full 78 parameter Helmholtz free-energy fit to the steam tables developed by Keenan et al. (1969). We also used the rigorous equations for the thermal conductivity (k_f) and viscosity (μ) of water given by the IAPS (1975, 1977). The reactor was operated under conditions such that the water did not enter the two-phase region (Maharrey, 1998).

Chemical Kinetics

Overall reaction

$$CH_3COOH + 4H_2O_2 \rightarrow 2CO_2 + 6H_2O$$

Global rate law

$$r_A = -DC_A/Dt = -V(dC_A/dx)$$
$$= -Ae^{-Eq/RT}[C_{HOAc}]^n[C_{Peroxide}]^m$$

The input for this reactor model is the experimentally measured total mass flow rate ($\dot{m}$), inlet pressure (P_o), inlet temperature (T_o), nozzle diameter (D_n), inlet composition of acetic acid and hydrogen peroxide (C_{HOAc} and $C_{Peroxide}$, respectively), and the outer quartz capillary wall temperature profile [$T_w(x)$]. These parameters were entered into the model and the reactor conditions calculated. At Mach 0.3, in the exit converging nozzle, the model switched over to the isentropic flow calculation and continued until the fluid velocity equaled the local speed of sound ($M = 1$). At this point, the nozzle diameter was calculated and compared to the measured value to assure that this was an accurate model calculation for the given experimental conditions. There is a direct relation between the fluid properties, the mass-flow rate, and the exit sonic nozzle diameter that must be consistent with the numerical calculations. This relation is sufficiently sensitive such that it becomes an independent assessment of the heat-transfer calculation and the nozzle diameter measurement. The calculated conversion of acetic acid is then compared with the experimentally measured conversion, and the parameters in the global rate law are adjusted until the model calculates the same conversion as is experimentally measured under the same conditions.

Table 1. Pure Water Results

P_{O1} (MPa)	$\dot{Q}$ (mL/h)	T_{O2} (°C)	$D_{N,calc}$ (μm)	$D_{N,meas}$ (μm)	T^*_{O2} (°C)
23	60	408	15.6	15	397
23	60	432	18.3	17.5	419
23	60	465	21.1	20.1	456
23	60	484	23.3	22	474
23	60	532	27.3	25.2	523

Results and Discussion

The first experiments completed were designed to test the heat-transfer model's calculation of the temperature of the water as it flowed through the reactor. For this test, we ran pure water through the reactor at various conditions and simulated these same experimental runs with the model. A comparison of the experimental runs with the model's calculated results for these runs would give an indication as to how well our heat-transfer model was predicting the reactor outlet temperature, temperature at the end of the constant area heating section, which also corresponds to the inlet temperature for the converging nozzle section. These results are shown in Table 1, where we show the reactor inlet pressure and total volumetric flow rate in columns 1 and 2, together with the model's calculation of the reactor outlet temperature (T_{02}), just before the flow enters the converging nozzle at station 2 in Figure 2, in column 3. The reactor outlet temperature, called the nozzle stagnation temperature in the compressible flow literature (Anderson, 1990), is the entrance temperature to the isentropic compressible flow section of the model. The model then calculates the nozzle diameter required to reach sonic flow at the nozzle, where the fluid velocity equals the local speed of sound, by an isentropic flow in a converging tube at a given inlet temperature (T_{02}). This calculated nozzle diameter is shown in column 4, and the independently measured experimental nozzle diameter is shown in column 5. If these two values do not match, as they should if the model has calculated the correct reactor outlet temperature (T_{02}), then the model steps back to the inlet of the isentropic nozzle section and perturbs the inlet temperature and recalculates the nozzle diameter. This perturbation is continued until the calculated and measured nozzle diameters agree. Column 6 shows the calculated inlet temperature (T^*) required by the isentropic nozzle section to match the calculated nozzle diameter to the measured diameter. Assuming the nozzle diameter is accurately known, this is also the reactor outlet temperature that should have been calculated by the heat-transfer section of the model.

With the reactor inlet pressure and total mass-flow rate both accurately known for these experiments, the heat-transfer model should be able to correctly calculate the reactor outlet temperature required by the isentropic nozzle section to calculate the correct sonic nozzle size ($D_{N,Calc} = D_{N,Meas}$). What the model instead showed was that for the heat-transfer section's calculated reactor outlet temperature, the sonic nozzle diameter needed to throttle this flow was 4–8% ($\sim$ 1.5–2 μm) larger than the measured nozzle diameter. If the isentropic nozzle section of the model was forced to reach sonic conditions for the measured diameter, then this calculation indicated that the reactor outlet temperature should

be lower by ~10°C than calculated by the heat-transfer section of the model. This result leads to two possibilities: either the measurement of the nozzle diameter was incorrect or the heat-transfer section of the model was overestimating the reactor outlet temperature. We know that the nozzle measurement technique we used proved to be accurate and reproducible to within ± 0.8 μm (0.00008 cm) for our conditions. Although it is likely that both errors contribute, the above results show that the heat-transfer model could be overestimating the reactor exit temperature of the fluid by, at most, 10°C. We feel this uncertainty represents a maximum uncertainty in the reactor temperature.

Figure 2 shows a typical reactor model simulation. An identical calculation was made for each experiment described below, and the kinetic parameters varied until the least-square residuals were minimized. In Figure 2, the temperature profile and the fractional conversion along the length of the reactor is shown. It is clearly shown that the reaction does not initiate until near the end of the reactor ($T_o > 470$°C) and then rapidly proceeds. Most of the reaction does appear to occur within a nearly isothermal region of the reactor, a fact that permitted us to estimate some kinetic parameters before we applied the rigorous analysis below. The nozzle is represented in the figure by the rapid drop in temperature over the very short distance beyond the 20 cm length of the reactor section. It is noted that the maximum conversion shown in the figure corresponds to the outlet of the reactor heating section at station 2 and that no further conversion was obtained within the nozzle section (2-3). For this particular calculation, the heat release from the reaction was minimal at such a small conversion ($< 10\%$) and resulted in the temperature profile without reaction deviating only about 0.3% from the profile with reaction and was therefore not included on this plot. As we mentioned above, the top of the figure shows the reactor and the four main locations identified: inlet (1), reactor (1-2), nozzle (2-3), and free-jet (3-Products). The free-jet region is not important in this discussion, but does come into play in the DSMS experiments to be discussed elsewhere, and is only mentioned for completeness. The typical residence time (τ) between states and the corresponding Reynolds number (Re) at each location are shown at the bottom of the figure. The rapid quenching of the reaction products is due to the very short flow times (2-3-Products) compared to the chemical reaction time. For comparison, the typical first-order reaction rate time constant for these reactions was on the order of 1–10 seconds. C_{ao} and C_{zo} give the initial acetic acid and hydrogen peroxide concentrations, respectively, used in this calculation.

The experiments were divided into two groups. Group I was used to analyze the Arrhenius rate constant parameters and consisted of experimental runs with changing reactor outlet temperature with all other conditions held constant. Group II was used to analyze the reactant orders in the rate law and consisted of experimental runs using different reactant initial concentrations with all other parameters held constant. Within a group, several different sets of experiments were run with a set defined as the experiments run at varying conditions under a single 250 mL water loading of the Varian high-pressure pump. A single run actually consists of from 3–5 identical runs in rapid succession, with the average of the individual conversions representing the true conversion for that run and the standard deviation in that average being the experimental error for the run. If a given planned set could not be completed within a single run of the Varian pump, then that set would be continued over to another complete 250 mL run of the Varian pump. The final run from the 250 mL load was repeated as the first run with the second 250 mL load and the set then continued. The range of conditions used for all the experimental sets were: reactor outlet temperatures from 450–500°C; initial acetic acid concentrations of 2, 5 and 10 wt. %; initial hydrogen peroxide concentrations of 1/8, 1/4, 1/2, 1, 2, and 4 times the stoichiometric concentration for a given run. All of the experimental sets were run at a fixed reactor pressure of 25 MPa and several were repeated at 23 and 28 MPa. Reactors used for these experiments had a range of nozzle exit diameters of from 15–25 μm, with most sets using reactors with diameters in the range of 18–20 μm. Two reactors were used with nozzle diameters of 12 and 27 μm.

Figure 3 shows a typical plot of the % conversion calculated by the model vs. the experimentally measured % conversion for the same reactor conditions from a single experimental set representing the variation of initial reactant concentrations. In this fit, the Arrhenius parameters of the model are held fixed; the Arrhenius parameters initially reported by Lee et al. (1990) are used here, but then iterated as discussed below. The figure shows the results for varying the reaction order of the acetic acid or oxidizer concentration with the order of the other reactant fixed. The data points shown in the plot represent the best-fit calculation and are spread around the 1:1 line, which would indicate a perfect fit outside the range of experimental uncertainty. Uncertainty in the calculated reaction order is shown in the figure by the upper and lower lines. These lines represent the maximum variation in either reaction order, while holding the other constant, which would fall outside the range of experimental uncer-

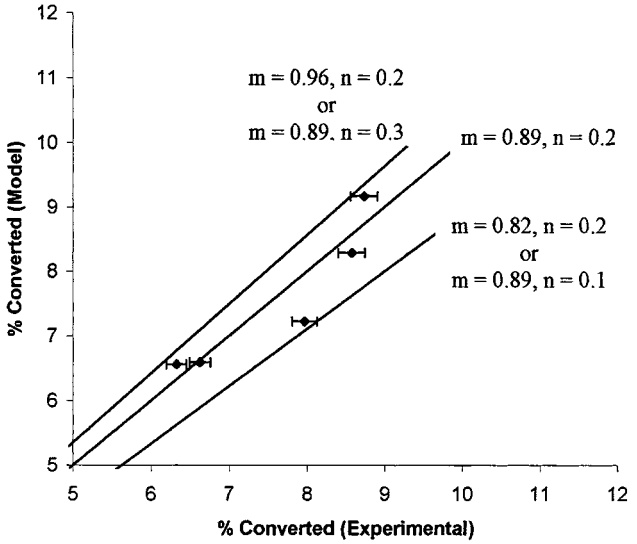

Figure 3. Model fit of reactant orders in global rate law to experimental data.

Acetic acid Order is given by m; Hydrogen Peroxide Order is given by n.

tainty. Again, the data points shown here are for one experimental set; we have data for well over 30 experimental sets, but are just showing the analysis results obtained for one set. Each individual data point in this set represents the average conversion obtained from five identical runs, while the error in each point is simply the standard deviation (at 68% confidence) of that average. The optimal value for the acetic acid order was determined in this way to be 0.89 ± 0.07, while the hydrogen peroxide order was determined to be 0.2 ± 0.1.

After the reactant concentration orders were estimated, a second data set was used to optimize the Arrhenius parameters. This data set represented experiments where all reactor conditions were held constant except the temperature. In this analysis, the concentration orders were held at the optimum values calculated and shown as above. Once the Arrhenius parameters were calculated from this second experimental data set, they were then reapplied to the order parameter data set above, used to calculate the concentration orders. This iteration was done to show the improvement obtained in the overall fit by optimizing the Arrhenius parameters. Figure 4 shows the results of this new fit of the optimized Arrhenius parameters on the earlier fit for the optimized reactant concentration orders shown in Figure 3. This new fit has improved the relative error of each individual data point and the overall fit (Figure 4) now deviates from the experimental by no more than 8% while the earlier fit (Figure 3) deviated by as much as 10%. The uncertainty in the Arrhenius parameters are obtained as above, for the reaction orders, and again shown by the upper and lower lines in Figure 4.

The final results calculated by the above procedure were an activation energy (E_a) of 172.2 ± 1.7 kJ/mol and a pre-exponential (A) of $9.3 \pm 0.7 \times 10^{10}$ $M^{-0.09}/s$ with reactant orders calculated to be 0.89 ± 0.07 and 0.2 ± 0.1 for acetic acid and hydrogen peroxide, respectively. Substituting these values into the power law model for the rate of reaction for acetic acid oxidation, the following form was obtained

$$r_A = -9.3 \pm 0.7 \times 10^{10} e^{-(172.2 \pm 1.7)/RT} [C_{\mathrm{HOAc}}]^{0.89 \pm 0.07} [C_{\mathrm{Peroxide}}]^{0.2 \pm 0.1} (\mathrm{M/s})$$

These values are still within the range of the published literature listed in the Li et al. (1991) article. Several investigators have assumed first-order kinetics for acetic acid and zeroeth-order for the oxidizer and then fit the Arrhenius parameters. In this way, Lee calculated an activation energy of 167.7 kJ/mol with a pre-exponential of 2.63×10^{10} s^{-1}, while Wilmanns (1990) calculated an activation energy of 131 kJ/mol with a pre-exponential of 9.23×10^{7} s^{-1}. By comparison, Wightman's (1981) data using oxygen as the oxidizer, when first-order in acid and zeroeth-order in oxidizer was assumed, yielded an activation energy of 172.7 kJ/mol and a pre-exponential of 2.55×10^{11} s^{-1}.

Later, experiments by Savage and Smith (1995) and Meyer et al. (1995), using oxygen as the oxidizer, did fit both reaction order and Arrhenius parameters, as we have done in the present experiments. It is difficult to compare with Savage and Smith, because they included water as a third species in the global kinetic model. Savage's calculations yielded a rate law first-order in acetic acid and 0.6 order in oxygen with an

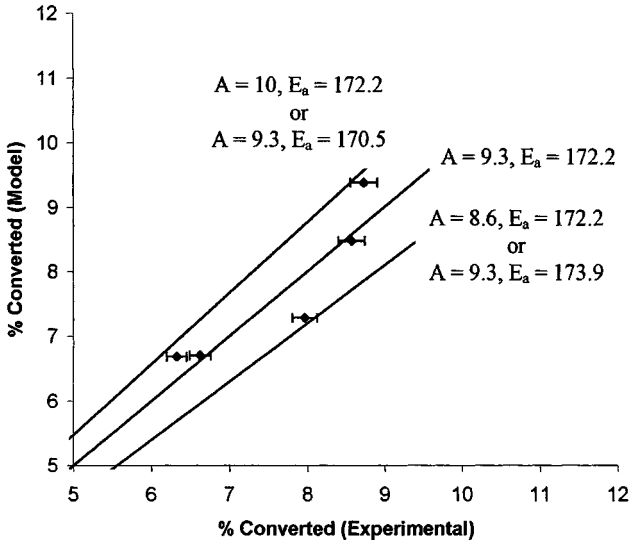

Figure 4. Model fit of Arrhenius rate constant parameters to experimental data set.

Where $k = A^* e^{-Eq/RT}$, $A^* = A \cdot 10^9$ s^{-1} and E_a is in kJ/mol.

activation energy of 307.9 kJ/mol and a pre-exponential of 6.3×10^{19} $M^{-2.6}/s$, and the water dependence was calculated as second-order. Meyer calculated a rate law 0.72 ± 0.15 order in acetic acid and 0.27 ± 0.15 order in oxygen with an activation energy of 168 ± 21 kJ/mol and a pre-exponential of $10^{9.9 \pm 1.7}$ $M^{0.01}/s$. Overall, we feel that the parameters we report here compare well with the data of Lee and of Meyer. We feel this analysis shows that the flexible microreactor design we report here can provide very useful kinetic data.

There exist two problems with our reactor design that need to be addressed to produce more reliable data and a more durable reactor. The quartz capillary has a limited useful lifetime due to thermal fatiguing and did not seem suitable much above 500°C. Supercritical water also has a finite, although very low, solubility for quartz. This later issue is one reason why the exit nozzle diameter was verified before and after each run, since the solubility effect is most significant on the small nozzle exit diameter, which controls the flow rate. Typically, the nozzle diameter would increase by one micron in 20 h of run time. The thermal fatiguing is the more serious issue, and we find that the useful lifetimes can be as long as 20 h before a new capillary must be used. In this sense, these microreactors are viewed as inexpensive ''throw away'' reactors.

The more serious challenge for the kinetic data is to make a more direct temperature measurement. While we feel confident of the heat-transfer calculation results that we have used, it is desirable to measure the reactant temperature directly. We could, of course, place the microreactor in a sand bath and assure that the reactor reaches an isothermal condition where most of the reaction occurs, as has been done with larger reactors. The advantages of flexibility and small power would still be available in such a geometry. We are also investigating the use of thicker-walled quartz tubing which would permit us to drill into the wall and cement in rigidly mounted thermocouples. Our heat-transfer calcula-

tions suggest that quartz walls can be increased substantially without affecting the heating power significantly. Thicker walled quartz tubing would be stronger and reduce the fatigue problem we observed with the thin-walled capillary tubing.

Conclusions

The design of a small-scale capillary quartz reactor for the investigation of SCWO reactions was developed. This reactor design provides a significant reduction in the energy density and mass flow rates required to reach supercritical conditions. The design is inexpensive and easy to repair after the failure of any given part. The reactor itself is simply a segment of capillary quartz with a nozzle of nominally 20 μm in diameter, obtained by simply melting the end of the quartz down in a methane/oxygen flame. The lifetime of a given quartz reactor can be 20 h, while the rest of the reactor assembly had a nominal lifetime of up to 300 h, before the nichrome heating loops would eventually fail. We also found that during the 20 h of runtime with a given quartz reactor, the diameter would increase by no more than 1 μm, and thus the eventual failure of the reactor was due to thermal fatigue and not clogging or erosion of the nozzle itself.

Because of the capillary design, standard instrumentation can be utilized directly, such as an HPLC pump and switching valves for introduction of different initial reactant loads during a single reactor run. A bypass segment is included for flushing the reactor of water after a run and also allowed for the measurement of the nozzle diameter both before and after each set of experimental runs. The heat-transfer model required to analyze the experimental data from the nonisothermal reactor was tested on pure water runs and proved to be able to accurately calculate the reactor exit temperature to better than 10 K out of 770 K.

The oxidation of acetic acid with hydrogen peroxide in supercritical water was chosen as the prototypical reaction to verify the reactor design. A set of experimental conditions was run and the experimental data, including operating conditions of the reactor and the reactor effluent, was collected. The recovered reactor effluent was analyzed to measure the conversion of acetic acid, and the calculated kinetic parameters are compared with available literature values.

In addition to being a flexible, low power reactor design, a major advantage is that the entire reactant effluent can be sampled directly, rather than by drawing off samples. Further, this design permits the integration of the reactor directly into a mass spectrometer vacuum system, which allows the mass spectrometer to be used as an online, real-time detection method for following the intermediate and radical species formed during SCWO. As mentioned above, the results of this direct sampling mass spectrometry detection system is currently in preparation (Maharrey and Miller, 2001).

Notation

a_S = fluid speed of sound, cm/s
A = Arrhenius pre-exponential factor, M^x/s
A_t = cross-sectional area of tube, cm
C_{HOAc} = concentration of acetic acid, mol/cm^3
$C_{Peroxide}$ = concentration of hydrogen peroxide, mol/cm^3
D_i = tube inlet diameter, cm
D_N = nozzle diameter, cm
D_o = tube outer diameter, cm
E_a = Arrhenius activation energy, kJ/mol
f_r = friction factor
h = fluid enthalpy, J/g
h_f = fluid heat-transfer coefficient, W/m$^2\cdot$K
k_f = water thermal conductivity W/m$\cdot$K
k_s = quartz capillary thermal conductivity W/m$\cdot$K
M = local Mach number, $M \equiv V/a_S$
M_i = molecular weight of species i, g/mol
Nu = fluid Nusselt number ($Nu \equiv h_f D/k_f$)
P = fluid pressure, J/cm^3
r_A = rate of reaction of acetic acid, mol/cm$^3\cdot$s
R = universal gas constant, J/mol$\cdot$K
Re = fluid Reynolds number, $Re \equiv \rho VD/\mu$
T = fluid temperature, °C
$T_w(x)$ = temperature profile along outer surface of capillary quartz, °C
U_T = overall heat-transfer coefficient, W/m$^2\cdot$K
V = fluid velocity, cm/s
x = reactor axial distance, cm
$\Delta H_R(T)$ = heat of reaction for acetic acid oxidation, J/mol
$\dot{m}$ = fluid mass-flow rate, g/s
$\dot{Q}$ = volumetric flow rate (mL/h)
ρ = fluid density, g/cm^3
ρ_i = species density, g/cm^3
μ = viscosity of water, g/cm$\cdot$s
ν_i = stoichiometric coefficient for species i

Literature Cited

Anderson, J. D., *Modern Compressible Flow*, McGraw Hill, New York and San Francisco (1990).

Aki, S. N. V. K., and A. Abraham, "An Economic Evaluation of Catalytic Supercritical Water Oxidation," *Environm. Prog.*, **17**, 246 (Winter, 1998).

Arpaci, V. S., and P. S. Larsen, *Convection Heat Transfer*, Prentice-Hall, Englewood Cliffs, NJ (1984).

Bird, R. B., W. E. Stewart, and E. N. Lightfoot, *Transport Phenomena* Wiley, New York (1960).

Brown, M. S., and R. R. Steeper, "CO_2-Based Thermometry of Supercritical Water Oxidation," *Appl. Spec.*, **45**, 1733 (1991).

Cansell, F., P. Beslin, and B. Berdeu, "Hydrothermal Oxidation of Model Molecules and Industrial Wastes," *Environm. Prog.*, **17**, 240 (Winter, 1998).

Cutler, A. H., M. J. Antal, Jr., and M. Jones, Jr., "A Critical Evaluation of the Plug-Flow Idealization of Tubular-Flow Reactor Data," *Ind. Eng. Chem. Res.*, **27**, 691 (1988).

Fukuoka, H., T. Imasaka, and N. Ishibashi, "Supercritical Fluid for Sample Introduction in Supersonic Jet Spectrometry," *Anal. Chem.*, **58**, 375 (1986).

Groeger, W., and J. B. Fenn, "Microjet Burners for Molecular-Beam Sources and Combustion Studies," *Rev. Sci. Instrum.*, **59**, 1971 (1988).

Lyon, D., "Supercritical Water Oxidation Offers Viable Alternative to Incinerator Upgrade," *Haz. Waste Consult.*, **17**, A1.11 (Jan.-Feb., 1999).

Holgate, H. R., and J. W. Tester, "Fundamental Kinetics and Mechanics of Hydrogen Oxidation in Supercritical Water," *Combust. Sci. Tech.*, **88**, 369 (1993).

IAPS, "Release on Surface Tension of Water Substance," H. J. White, Secr., International Association for the Properties of Steam, Nat. Bur. Stand., Washington, DC (1975).

IAPS, "Release on Static Dielectric Constant of Water Substance," H. J. White, Secr., International Association for the Properties of Steam, Nat. Bur. Stand., Washington, DC (1975).

Keenan, J. F., F. G. Keyes, P. G. Hill, and J. G. Moore, *Steam Tables* Wiley, New York (1969).

Lee, D. S., E. F. Gloyna, and L. Li, "Efficiency of H_2O_2 and O_2 in Supercritical Water Oxidation of 2,4-Dichlorophenol and Acetic Acid," *J. Supercrit. Fluids*, **3**, 249 (1990).

Li, L., P. Chen, and E. F. Gloyna, "Generalized Kinetic Model for Wet Oxidation of Organic Compounds," *AIChE J.*, **37**, 1687 (1991).

Lustig, D. A., and D. M. Lubman, "A Continuous Flow Probe Method for On-Line Introduction of Liquid Samples for Detection by Laser

Desorption with Resonant Two-Photon Ionization in Supersonic Beam Mass Spectrometry,'' *Rev. Sci. Instrum.*, **62**, 957 (1991).
Maharrey, S. P., and D. R. Miller, ''A Direct Sampling Mass Spectrometer Investigation of Oxidation Mechanisms for Acetic Acid in Supercritical Water,'' *J. Phys. Chem.*, in press (2001).
Maharrey, S. P., ''A Study of the Oxidation of Acetic Acid in Supercritical Water Using a Micro-Reactor and Direct Sampling Mass Spectrometry,'' PhD Diss., Dept. of Applied Mechanics and Engineering Sciences, University of California, San Diego (1998).
Meyer, J. C., P. A. Marrone, and J. W. Tester, ''Acetic Acid Oxidation and Hydrolysis in Supercritical Water,'' *AIChE J.*, **41**, 2108 (1995).
Modell, M., ''Supercritical Water Oxidation,'' *Standard Handbook of Hazardous Waste Treatment and Disposal*, H. M. Freeman, ed., McGraw-Hill, New York (1989).
Myrick, M. L., J. Kolis, E. Parsons, K. Chike, M. Lovelace, W. Scrivens, R. Holiday, and M. Williams, ''In Situ Fiber-Optic Raman Spectroscopy of Organic Chemistry in a Supercritical Water Reactor,'' *J. Raman Spec.*, **25**, 59 (1994).
Randall, L. G., and A. L. Wahrhaftig, ''Dense Gas Chromatograph/Mass Spectrometer Interface,'' *Anal. Chem.*, **50**, 1703 (1978).
Randall, L. G., and A. L. Wahrhaftig, ''Direct Coupling of a Dense (Supercritical) Gas Chromatograph to Mass Spectrometer using a Supersonic Molecular Beam Interface,'' *Rev. Sci. Instrum.*, **52**, 1283 (1981).
Rice, S. F., R. R. Steeper, and C. A. LaJeunesse, ''Destruction of Representative Navy Wastes Using Supercritical Water Oxidation,'' Sandia National Lab. Rep. No. SAND94-8203 (1993).
Rice, S. F., T. B. Hunter, A. C. Ryden, and R. G. Hanush, ''Raman Spectroscopic Measurement of Oxidation in Supercritical Water: 1. Conversion of Methanol to Formaldehyde,'' *Ind. Eng. Chem. Res.*, **35**, 2161 (1996).
Rice, S. F., and R. R. Steeper, ''Oxidation Rates of Common Organic Compounds in Supercritical Water,'' *J. Haz. Mat.*, **59**, 261 (Apr. 1998).
Savage, P. E., and M. A. Smith, ''Kinetics of Acetic Acid Oxidation in Supercritical Water,'' *Environ. Sci. Technol.*, **29**, 216 (1995).
Schmieder, H., and J. Abeln, ''Supercritical Water Oxidation: State of the Art,'' *Chem. Eng. Technol.*, **22**, 903 (Nov., 1999).
Smith, R. D., J. L. Fulton, R. C. Petersen, A. J. Kopriva, and B. W. Wright, ''Performance of Capillary Restrictors in Supercritical Fluid Chromatography,'' *Anal. Chem.*, **58**, 2057 (1986).
Syage, J. A., ''Real-Time Detection of Chemical Agents Using Molecular Beam Laser Mass Spectrometry,'' *Anal. Chem.*, **62**, 505A (1990).
Tester, J. W., H. R. Holgate, F. J. Armellini, P. A. Webley, W. R. Killilea, G. T. Hong, and H. E. Barner, ''Oxidation of Hazardous Organic Wastes in Supercritical Water: A Review of Process Development and Fundamental Research,'' *ACS Symp. Ser. 518: Emerging Technologies in Hazardous Waste Management III*, D. W. Tedder and F. G. Pohland, eds., Amer. Chem. Soc. (1993).
Wightman, T. J., ''Studies in Supercritical Wet Air Oxidation,'' MS Thesis, Univ. of California, Berkeley (1981).
Wilmanns, E. G., ''Supercritical Water Oxidation of Volatile Acids,'' MS Thesis, Civil Eng. Dept., Univ. of Texas, Austin (1990).
Yamagata, K., K. Nishikawa, S. Hasegawa, T. Fujii, and S. Yoshida, ''Forced Convective Heat Transfer to Supercritical Water Flowing in Tubes,'' *Int. J. Heat Mass Transfer*, **15**, 2575 (1972).

Manuscript received Aug. 7, 2000, and revision received Nov. 8, 2000.